

ORIGINAL ARTICLE

Catalyst-free growth of InAs/In_xGa_{1-x}As coaxial nanorod heterostructures on graphene layers using molecular beam epitaxy

Youngbin Tchoe¹, Janghyun Jo², Miyoung Kim² and Gyu-Chul Yi¹

We report the catalyst-free growth of InAs/In_xGa_{1-x}As coaxial nanorod heterostructures on large-area graphene layers using molecular beam epitaxy and our investigation of the chemical composition and crystal structure of these heterostructures using electron microscopy. The graphene layers used as the substrate were prepared by chemical vapor deposition and transferred onto SiO₂/Si substrates. InAs nanorods and their heterostructures were grown vertically on the graphene layers; electron microscopy images revealed uniform distributions for their diameter, length and density. Cross-sectional electron microscopy images showed that In_xGa_{1-x}As layers, having uniform composition, coated heteroepitaxially the entire surface of the InAs nanorods, without interfacial layers or structural defects. The catalyst-free growth mechanism of InAs nanorods on graphene was investigated using *in situ* reflection high-energy electron diffraction.

NPG Asia Materials (2015) 7, e206; doi:10.1038/am.2015.88; published online 7 August 2015

INTRODUCTION

The use of inorganic semiconductors as an active material is desirable for flexible electronic and optoelectronic device applications,¹⁻³ due to the many potential advantages over organic semiconductors in terms of lifetime and efficiency.⁴ However, continuous, rigid inorganic semiconductor thin films have no tolerance for mechanical deformation. To address this issue, direct growth of semiconductor nanorods on graphene that has high mechanical strength and flexibility was demonstrated recently, mainly using metal-organic chemical vapor deposition;⁵⁻⁷ for example, flexible light-emitting diodes and solar cells using metal-organic chemical vapor deposition-grown GaN and InGaAs nanorods on graphene.⁸⁻¹¹ Nevertheless, molecular beam epitaxy (MBE) can provide accurate control over the growth parameters for high-quality nanorod heterostructures with very clean and sharp interfaces using various *in situ* monitoring techniques, such as reflection high electron energy diffraction (RHEED).^{12,13} Realizing the advantage of MBE growth method, Zhuang *et al.* demonstrated In droplet-assisted growth of InAs nanorods on mechanically exfoliated graphite flakes using MBE.¹⁴ However, it is important to develop catalyst-free MBE growth method of nanorods on graphene, as this growth method is known to be the best method to produce ultrapure nanorods with homogeneous composition, which are essential building blocks for future nanorod-based devices.¹⁵ Here we demonstrate the growth of high-quality InAs/In_xGa_{1-x}As coaxial nanorod heterostructures on graphene layers using MBE, with a clean interface. Both transmission electron microscopy (TEM) and *in situ* RHEED

were used to investigate the structural properties and growth mechanism of the nanorod heterostructures.

MATERIALS AND METHODS

Preparation of graphene films

Chemical vapor deposited (CVD) large-area graphene layers were prepared as substrates for InAs nanorods and InAs/In_xGa_{1-x}As coaxial nanorod heterostructures growth. To prepare large-area graphene substrates, graphene films were synthesized on copper foil via CVD, and then transferred onto amorphous SiO₂-covered Si (SiO₂/Si) substrate supports.⁸ Raman spectroscopy and cross-sectional TEM confirmed the successful preparation of graphene layers and their number ($n = 10$). Before loading of the graphene substrates inside the MBE growth chamber, polymer residue on the substrates was removed by thermal decomposition at 530 °C for 1 h inside an ultrahigh-vacuum preparation chamber.

Molecular beam epitaxial growth of InAs/In_xGa_{1-x}As coaxial nanorod heterostructures on graphene layers

In this study, we used a two-step MBE process: (i) high-temperature synthesis of ultrafine-core InAs nanorods, and (ii) subsequent low-temperature coating of In_xGa_{1-x}As shell layers on the InAs core nanorods for fabrication of InAs/In_xGa_{1-x}As coaxial nanorod heterostructures on graphene layers. This two-step MBE growth method was employed to produce In_xGa_{1-x}As shell layers with precisely controlled chemical composition and thickness, which resulted in highly controlled nanorod heterostructures with clean interface compared with spontaneous phase separated metal-organic chemical vapor deposition-grown InAs core and In_xGa_{1-x}As shell nanowires.⁷ Inside of a cryogenically cooled ultrahigh-vacuum growth chamber (RIBER 32P), InAs nanorods were grown at 530 °C for 1 h, by supplying high-purity indium

¹Department of Physics and Astronomy, Institute of Applied Physics, Seoul National University, Seoul, Korea and ²Department of Materials Science and Engineering and Research Institute of Advanced Materials, Seoul National University, Seoul, Korea
Correspondence: Professor G-C Yi, Department of Physics and Astronomy, Institute of Applied Physics, Seoul National University, Seoul 151-747, Korea.
E-mail: gcyi@snu.ac.kr

Received 27 January 2015; revised 11 June 2015; accepted 15 June 2015

(In) and uncracked arsenic (As₄) molecular beams from Knudsen cells. The beam-equivalent pressures (BEPs) of In and As₄ were 6×10^{-8} and 7×10^{-5} Torr, respectively. For catalyst-free growth of InAs nanorods, we supplied As₄ to the substrates for 10 min before supplying In to prevent In droplet formation on the graphene layers, which resulted in quite different nucleation and crystal growth behavior from vapor–liquid–solid (VLS) growth.^{14,16}

After the preparation of InAs nanorods, InAs/In_xGa_{1-x}As coaxial nanorod heterostructures were subsequently synthesized by heteroepitaxial growth of an In_xGa_{1-x}As thin layer on InAs core nanorods. Deposition of In_xGa_{1-x}As coaxial shell layers was performed at 380 °C for 1 h by the addition of a gallium (Ga) molecular beam, resulting in an In_xGa_{1-x}As layer coating over the entire InAs nanorod surface. For the growth of In_xGa_{1-x}As coaxial shell layers, In, Ga and As₄ BEPs that we used were 6×10^{-8} , 1×10^{-8} and 2×10^{-6} Torr, respectively. Because the molecular beam fluxes were strongly one-directional, the vertically well-aligned nanorods were placed on rotating substrates to allow uniform exposure to all sides of the nanorods by the molecular beam fluxes; this resulted in homogeneous, uniform film formation, in terms of thickness and composition of the coaxial shell layers.

RHEED and TEM characterizations

The entire growth procedure was monitored *in situ* via RHEED (electron beam energy: 22.2 keV; spot size: 0.2 mm). The length of the electron-beam irradiated area along the beam trajectory was 15 mm, indicating a 1° incident angle of the electron beam with respect to the substrate surface. Real-time video of the RHEED patterns was acquired using a commercial digital single-lens reflex camera; the time resolution of the video was 0.04 s. The lattice parameters of the InAs nanorods and CVD graphene layers were estimated by comparing the spacing between RHEED patterns with that of Si(111) substrates as a reference. RHEED images during the coaxial shell-layer growth were acquired by temporarily stopping the growth by closing In and Ga shutters and rotation of the substrates.

For detailed structural analysis, the cross-section of the InAs/In_xGa_{1-x}As coaxial nanorod heterostructures was prepared by dual-beam focused ion beam (FIB) milling and analyzed using TEM. The chemical composition was analyzed by high-angle annular dark-field scanning TEM (STEM) equipped with energy dispersive X-ray spectroscopy (STEM–EDS) capabilities. In addition, the

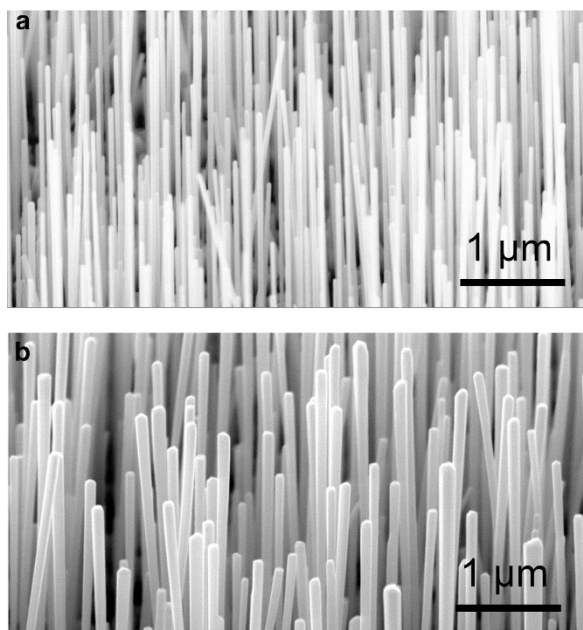


Figure 1 Scanning electron microscopy tilted images of (a) InAs nanorods grown on CVD graphene layers and (b) InAs/In_xGa_{1-x}As coaxial nanorod heterostructures grown on CVD graphene layers.

InAs/In_xGa_{1-x}As coaxial nanorod heterostructure crystallinity was investigated by bright-field and high-resolution (HR) TEM.

To characterize crystal structure of the InAs/In_xGa_{1-x}As coaxial nanorod heterostructures, HR-TEM images were taken near the zone axis of $(10\bar{1}0)_{\text{WZ}} \parallel (2\bar{1}\bar{1})_{\text{ZB}}$ that is perpendicular to the growth direction (see Supplementary Figure S4). To prepare this sample, InAs/In_xGa_{1-x}As coaxial nanorod heterostructures with 5-nm-thick In_xGa_{1-x}As layers were prepared, ultrasonically dispersed in ethanol anhydrous, and subsequently drop-casted and dried on TEM grids.

RESULTS AND DISCUSSION

MBE growth of InAs/In_xGa_{1-x}As coaxial nanorod heterostructures on graphene layers

The surface morphologies of InAs nanorods and InAs/In_xGa_{1-x}As coaxial nanorod heterostructures grown on CVD graphene layers were investigated using scanning electron microscopy. The tilted scanning electron microscopy image in Figure 1a shows that the high-density InAs nanorods were vertically well aligned on the graphene layers. The mean diameter, height and density of the InAs nanorods were 70 nm, 10 μm and $5 \times 10^8 \text{ cm}^{-2}$, respectively. Meanwhile, Figure 1b shows a tilted scanning electron microscopy image of InAs/In_xGa_{1-x}As coaxial nanorod heterostructures on CVD graphene layers. After coaxial coating of the In_xGa_{1-x}As shell layer, the mean diameter of nanorods increased to 110 nm, indicating that the average thickness and growth rate of the In_xGa_{1-x}As shell layer was 20 nm and 0.06 \AA s^{-1} , respectively. Non-tapered morphology was also observed, indicating that the thickness of the In_xGa_{1-x}As shell layer was uniform over the entire surface. The surface morphology of the shell layer depended critically on the As₄ BEP; whereas, the uniform coating of the shell layer shown in Figure 1b was achieved for an As₄ BEP of 2×10^{-6} Torr, inverse-tapered shapes were observed for a higher As₄ BEP of 5×10^{-6} Torr or above (see Supplementary Figure S1).

We also investigated the critical growth parameters that affected the dimension and density of InAs nanorods (see Supplementary Figures S2 and S3). The diameter of the nanorods generally increased with In BEP (see Supplementary Figure S2c) and the height of the nanorods depended on both As₄ BEP and growth temperatures. S. Hertenberger *et al.* explained that, either at high As/In ratio near the InAs nanorod tip or at high growth temperature, diffusion length of In adatom increases and the probability for incorporation at the InAs nanorod growth front is enhanced compared with that at the lateral sidewalls.¹⁷ Meanwhile, the density of the InAs nanorods depended on both molecular fluxes and growth temperature, as these factors strongly affect the surface migration lengths of adatoms.^{17,18}

RHEED characterization

In this study, MBE-grown InAs nanorods on CVD graphene layers were monitored *in situ* in the initial growth stage using RHEED. Before the nanorod growth, as shown in Figure 2a, a streaky RHEED pattern was observed from CVD graphene layers transferred onto a SiO₂/Si substrate. The streaky RHEED patterns of CVD graphene layers remained unchanged, regardless of the azimuthal rotation angles, which strongly suggests that the hexagonal graphitic layers were aligned in the (001) direction and the in-plane orientations of each grain were random. When the nanorod growth was initiated ($t=0$), the streaky RHEED pattern of CVD graphene layers (Figure 2a) was changed to bright Bragg spots corresponding to InAs nanorods (Figure 2b) within a few seconds of In-shutter opening. The appearance of these spots indicated an abrupt change from two-dimensional RHEED patterns to three-dimensional Bragg diffraction patterns.¹²

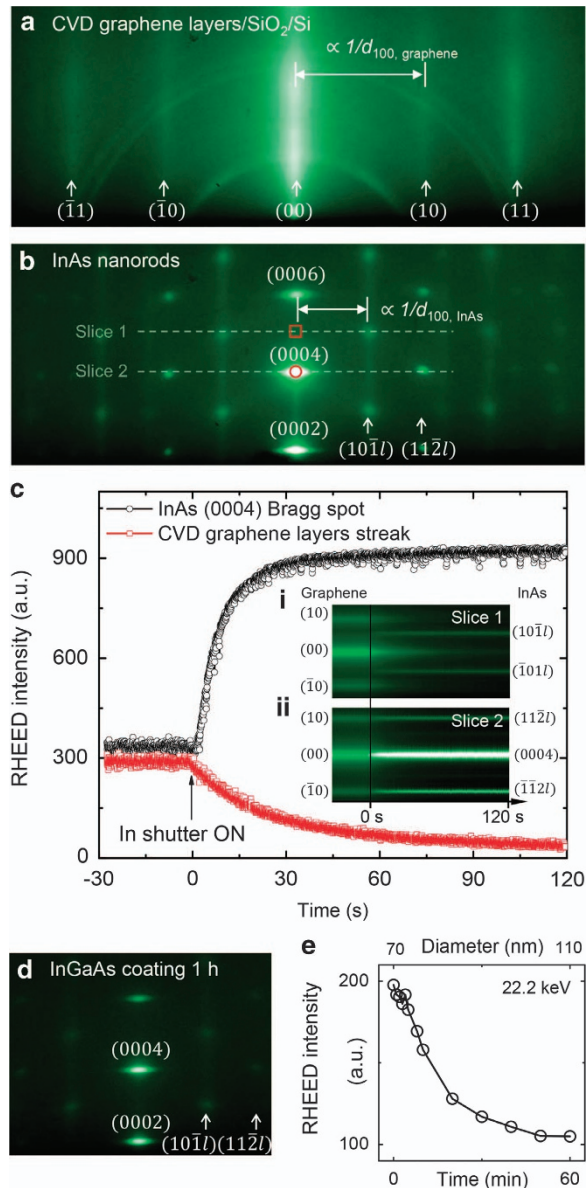


Figure 2 RHEED patterns during InAs/In_xGa_{1-x}As coaxial nanorod heterostructure growth on CVD graphene layers. RHEED patterns of (a) CVD graphene layers transferred onto SiO₂/Si substrates and (b) InAs nanorods grown on CVD graphene layers/SiO₂/Si. (c) Integrated RHEED intensities of (0004) InAs Bragg spots (red circle in b) and (00) streak from CVD graphene layers (red box in b) as a function of time. The inset shows the evolution of RHEED intensities along the dotted lines (i) slice 1 and (ii) slice 2 in b, plotted as a function of time. (d) RHEED patterns of InAs/In_xGa_{1-x}As coaxial nanorod heterostructures on CVD graphene layers, after growing 20-nm-thick In_xGa_{1-x}As coaxial shell layers. (e) Integrated RHEED intensity of (0004) InAs Bragg spot during the coaxial coating of In_xGa_{1-x}As shell layers.

To further examine the abrupt change in RHEED patterns, the integrated RHEED intensities of the InAs Bragg spot (circle in Figure 2b) and the streak from CVD graphene layers (rectangular box in Figure 2b) were plotted as a function of time in Figure 2c. An abrupt rise in the integrated RHEED intensity of the InAs (0004) Bragg spot was observed without delay (within 1 s), as shown in Figure 2c. The instantaneous, monotonic increase in the Bragg spot intensity, not observed typically for metal-catalyst-assisted VLS

growth mode,^{12,13} strongly suggests the direct formation of catalyst-free InAs nanorod crystal growth on CVD graphene layers.

In addition, the lattice parameters of the CVD graphene layers and InAs nanorods were estimated by comparing the spacing between the RHEED patterns, as indicated in Figures 2a and b. The d_{100} interplanar spacing of CVD graphene layers and wurtzite InAs nanorods were 2.1 and 3.7 Å, respectively, which is in agreement with the previously reported values.^{19,20} To examine the change in the lattice parameters during the initial growth stage, the evolution of RHEED intensities along the dotted lines in Figure 2b was plotted as a function of time in the combined images shown in the inset of Figure 2c. Inset (i) of Figure 2c clearly shows the (10 $\bar{1}$) Bragg spots of InAs that appeared abruptly with the initiation of growth ($t = 0$); the position of these spots did not change as growth progressed, implying that unstrained InAs nanorod crystals formed directly on CVD graphene layers, without a strain relaxation step. Inset (ii) of Figure 2c shows that the position of the (10) streak from CVD graphene layers was aligned indistinguishably with that of (11 $\bar{2}$) InAs Bragg spots, implying a possible in-plane, lattice-matching configuration of InAs crystals and graphene layers.^{16,21}

For longer growth times approaching 1 h and InAs nanorod lengths reaching 10 μm, sharp spots were clearly visible in the RHEED patterns (Figure 2b) thanks to the transmission mode of RHEED.²² For all azimuthal rotation angles, the RHEED patterns from the InAs nanorods were the same, indicating that the nanorods were vertically well aligned along [0002]_{WZ} and [111]_{ZB}, but their in-plane orientations were random; these results were attributed to in-plane misorientations of grains in the CVD graphene layers.^{19,23}

RHEED also enabled us to investigate the growth of In_xGa_{1-x}As coaxial shell layers as well as InAs nanorods. For In_xGa_{1-x}As coaxial-shell layer growth, although the RHEED intensity decreased with growth time as the nanorod thickness increased, no significant change in the RHEED pattern was observed, as shown in Figures 2d and e. From the fact that the RHEED patterns maintained the same shape during coaxial shell-layer growth, we suggest that the In_xGa_{1-x}As coaxial shell layer grew epitaxially on the InAs nanorods; this was later confirmed by cross-sectional TEM analysis.

Structural and chemical compositional analyses of InAs/In_xGa_{1-x}As coaxial nanorod heterostructures

The structural characteristics of InAs/In_xGa_{1-x}As coaxial nanorod heterostructures were investigated using TEM. As indicated in the schematic diagram, cross-sectional TEM samples were prepared using focused ion beam. Figure 3b shows a cross-sectional bright-field image of InAs/In_xGa_{1-x}As nanorods, exposing the (0001) surface. As the interface between the In_xGa_{1-x}As and InAs layers was indistinguishable in the bright-field image without performing chemical analysis, the interface between the In_xGa_{1-x}As shell layer and InAs nanorod core is indicated by dotted hexagonal lines in the figure by comparing STEM image and STEM-EDS mapping results, which will be later shown in Figure 4. Both the In_xGa_{1-x}As shell layer and the InAs core exhibited well-developed {11 $\bar{2}$ 0} facets, as opposed to {10 $\bar{1}$ 0} facets, verified exclusively by the fast Fourier transform (FFT) pattern in the inset of Figure 3b. This single type of facets were identically observed for 10 randomly selected nanorods. Previous TEM studies showed that both {10 $\bar{1}$ 0} and {11 $\bar{2}$ 0} side facets were present in the InAs nanorod system.^{24,25} However, formations of the only {11 $\bar{2}$ 0} facets for In_xGa_{1-x}As shell layer and InAs core may be associated with a smaller surface energy for the {11 $\bar{2}$ 0} side facet than that of the {10 $\bar{1}$ 0} side facet in the InAs nanorod.^{15,26} The epitaxial relationship and atomic structure of InAs/In_xGa_{1-x}As coaxial nanorod heterostructures were

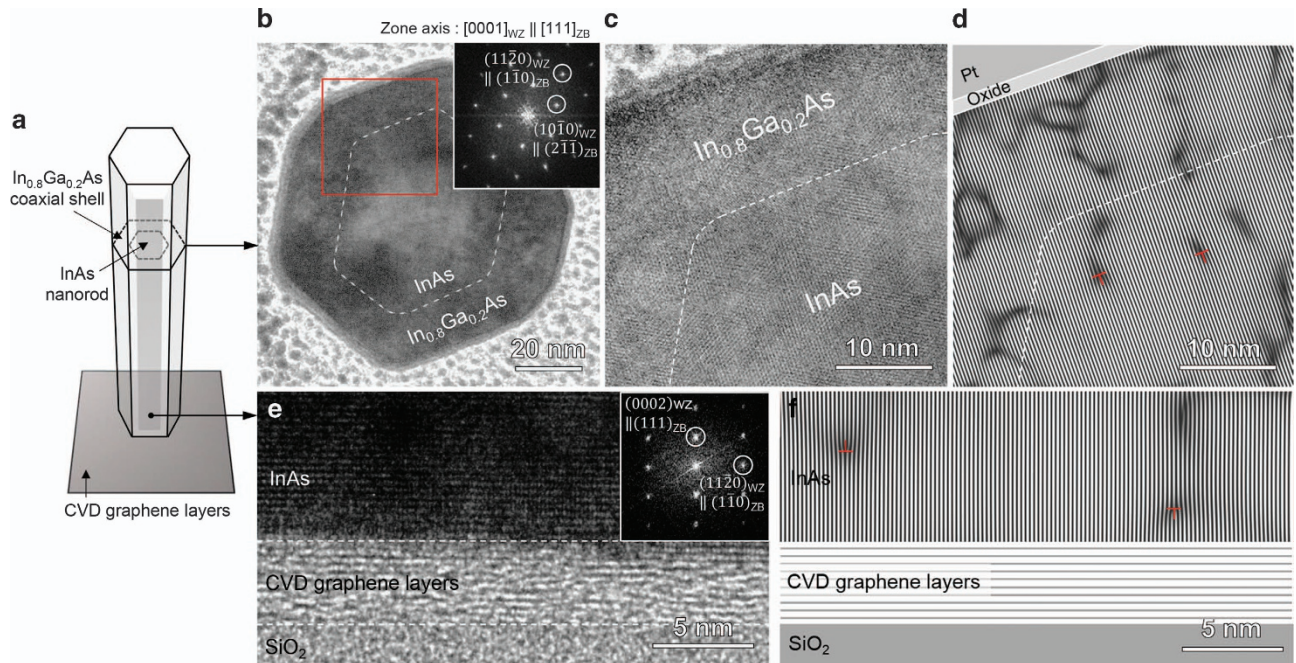


Figure 3 Microstructure of InAs/In_xGa_{1-x}As coaxial nanorod heterostructures on CVD graphene layers. (a) Schematic diagram of the TEM sampling positions and the corresponding plan-view (b) bright-field-TEM, (c) HR-TEM and (d) Fourier-filtered images of InAs/In_xGa_{1-x}As coaxial nanorod heterostructures. The inset diffraction patterns in (b) are obtained via FFT of the HR-TEM images in (c). The areas of oxide layer formed on the nanorod surface and Pt-protection layer are marked in (d). Cross-sectional (e) HR-TEM and (f) Fourier-filtered images of the interface between InAs and CVD graphene layers. The inset diffraction patterns in (e) were obtained via FFT of the corresponding HR-TEM image. The locations of misfit dislocations estimated by Fourier-filtered images are indicated by T.

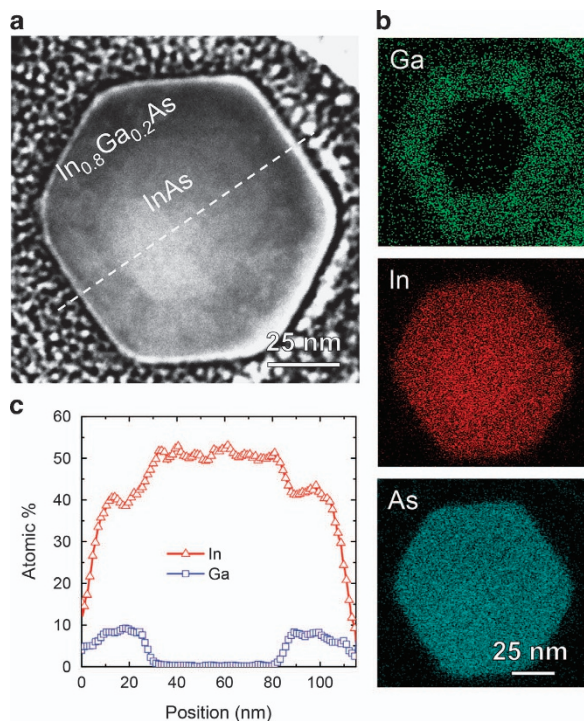


Figure 4 Chemical composition of InAs/In_xGa_{1-x}As coaxial nanorod heterostructures grown on CVD graphene layers. (a) Plan-view STEM image, (b) elemental mapping of Ga, In and As using STEM-EDS, and (c) EDS line profiles of In and Ga along the dotted line in (a).

investigated using HR-TEM. Figure 3c shows a HR-TEM image of the region marked with a rectangular box in Figure 3b. Significant edge dislocations were not observed at the interface between InAs and

In_xGa_{1-x}As layers. The interface in the coaxial nanorod heterostructures was further examined in more detail by the Fourier-filtered image shown in Figure 3d, obtained by selecting the (10 $\bar{1}$ 0) FFT spots of both InAs and In_xGa_{1-x}As. The areas of oxide layer formed on the nanorod surface and Pt-protection layer are also marked in Figure 3d. The Fourier-filtered image in Figure 3d shows fringe patterns were well aligned at the heterointerfaces with few misfit dislocations. The locations of misfit dislocations estimated by Fourier-filtered images are indicated by T. These TEM results strongly suggest that the growth of In_xGa_{1-x}As on InAs is coherently epitaxial, which results presumably from small lattice mismatch (<1%) between the InAs and In_xGa_{1-x}As layers. Such an epitaxial relationship with a small lattice mismatch produced nearly overlapped FFT patterns in the inset of Figure 3b.

We also investigated the atomic arrangement of InAs at the interface between InAs and graphene using cross-sectional HR-TEM images. Figure 3e shows a clean interface between the InAs nanorod and graphene layers without any interfacial layer. HR-TEM images of the InAs nanorod crystal in Figure 3e revealed a well-aligned growth direction, parallel to the *c* axis of CVD graphene, as indicated by FFT in the inset. Fourier filter analysis was also performed to investigate the microstructural characteristics of the InAs nanorod at the interface. Figure 3f is a Fourier-filtered image of Figure 3e, obtained by selecting the (11 $\bar{2}$ 0) FFT spots of InAs. This image reveals that the dislocations were not concentrated close to the interface; this outcome would be attributed to the heteroepitaxial relationship between the graphene layers and InAs.^{6,16,19}

The crystal structure of In_xGa_{1-x}As/InAs coaxial nanorod heterostructures was investigated by HR-TEM images near the zone axis of (10 $\bar{1}$ 0)_{WZ} || (2 $\bar{1}$ 1)_{ZB}, which clearly confirmed the existence of alternating zinc blende and wurtzite crystal phases both along the InAs nanorods and In_xGa_{1-x}As shell layers (see Supplementary Figure S4).

In addition to the structural analysis, the chemical composition of InAs/In_xGa_{1-x}As coaxial nanorod heterostructures was investigated by STEM and EDS. As shown in Figure 4a, from the contrast change in cross-sectional STEM image of a (0001) surface of an InAs/In_xGa_{1-x}As nanorod, which reflects difference in atomic mass of elements, hexagonal formation of InAs core was evidently observed in bright inner area, as well as the uniformly coated In_xGa_{1-x}As shell layer in dark outer area, indicating that heavier Ga atoms were incorporated at the shell layers. The STEM-EDS mapping of each element in Figure 4b clearly shows the spatial distribution of In, Ga and As. Ga existed only in the hexagonal ring-shaped outer-shell region; In was detected over the entire nanorod while having a higher density in the inner hexagonal core; and As was detected uniformly over the entire nanorod structure.

To quantify the chemical composition of each layer, we measured the STEM-EDS line profile along the dotted line in Figure 4a, which is plotted graphically in Figure 4c. From this result, we confirmed the formation of the InAs/In_xGa_{1-x}As coaxial nanorod heterostructure and chemical composition of the In_xGa_{1-x}As shell layer. A larger amount of In atoms, four-fold over that of Ga, was detected; thus, the *x* value of In_xGa_{1-x}As layer was 0.8 as estimated by STEM-EDS.

CONCLUSION

In conclusion, vertically well aligned, high-quality InAs/In_xGa_{1-x}As coaxial nanorod heterostructures were grown on CVD graphene layers using MBE. From *in situ* RHEED observation, we confirmed that the InAs nanorods grew on CVD graphene layers in a catalyst-free mode. The formation of InAs/In_xGa_{1-x}As coaxial nanorod heterostructures was confirmed by STEM and EDS analysis, which showed a clearly defined InAs core and In_xGa_{1-x}As shell layer with uniform composition and thickness. In addition, cross-sectional HR-TEM images demonstrated a clean interface between In_xGa_{1-x}As and InAs. Our work would provide a novel and straightforward pathway for a monolithic integration of semiconductor coaxial nanorod heterostructures on two-dimensional layered materials, which is a key factor to exploit it for flexible electronics and optoelectronics.

CONFLICT OF INTEREST

The authors declare no conflict of interest.

ACKNOWLEDGEMENTS

This work was supported by Seoul National University (SNU)-Yonsei Research Cooperation Program through SNU in 2014. This work was also supported by the Future-based Technology Development Program (Nano Fields) through the National Research Foundation (NRF) of Korea funded by the Ministry of Education, Science and Technology (MEST) (No. 2014M3A7B4051589, No. 2010-0029325 (0417-20140099) and NRF 2014023231). YT is grateful for the generous support of the TJ Park Science Fellowship program from the POSCO TJ Park Foundation.

- Ponce, F. & Bour, D. Nitride-based semiconductors for blue and green light-emitting devices. *Nature* **386**, 351–359 (1997).
- Kim, Y.-J., Lee, J.-H. & Yi, G.-C. Vertically aligned ZnO nanostructures grown on graphene layers. *Appl. Phys. Lett.* **95**, 213101 (2009).
- Hong, Y. J. & Fukui, T. Controlled van der Waals heteroepitaxy of InAs nanowires on carbon honeycomb lattices. *ACS Nano* **5**, 7576–7584 (2011).
- Mohseni, P. K., Behnam, A., Wood, J. D., English, C. D., Lyding, J. W., Pop, E. & Li, X. In_xGa_{1-x}As nanowire growth on graphene: van der Waals epitaxy induced phase segregation. *Nano Lett.* **13**, 1153–1161 (2013).
- Lee, C.-H., Kim, Y.-J., Hong, Y. J., Jeon, S. R., Bae, S., Hong, B. H. & Yi, G.-C. Flexible inorganic nanostructure light-emitting diodes fabricated on graphene films. *Adv. Mater.* **23**, 4614–4619 (2011).
- Kim, Y.-J., Yoo, H., Lee, C.-H., Park, J. B., Baek, H., Kim, M. & Yi, G.-C. Position- and morphology-controlled ZnO nanostructures grown on graphene layers. *Adv. Mater.* **24**, 5565–5569 (2012).
- Mohseni, P. K., Behnam, A., Wood, J. D., Zhao, X., Yu, K. J., Wang, N. C., Rockett, A., Rogers, J. A., Lyding, J. W. & Pop, E. Monolithic III-V nanowire solar cells on graphene via direct van der Waals epitaxy. *Adv. Mater.* **26**, 3755–3760 (2014).
- Chung, K., Beak, H., Tchoe, Y., Oh, H., Yoo, H., Kim, M. & Yi, G.-C. Growth and characterizations of GaN micro-rods on graphene films for flexible light emitting diodes. *APL Mater.* **2**, 092512 (2014).
- Hertenberger, S., Rudolph, D., Bolte, S., Döblinger, M., Bichler, M., Spirkoska, D., Finley, J., Abstreiter, G. & Koblmüller, G. Absence of vapor-liquid-solid growth during molecular beam epitaxy of self-induced InAs nanowires on Si. *Appl. Phys. Lett.* **98**, 123114 (2011).
- Rudolph, D., Hertenberger, S., Bolte, S., Paosangthong, W., Spirkoska, D., Döblinger, M., Bichler, M., Finley, J. J., Abstreiter, G. & Koblmüller, G. Direct observation of a noncatalytic growth regime for GaAs nanowires. *Nano Lett.* **11**, 3848–3854 (2011).
- Zhuang, Q. D., Anyebe, E. A., Sanchez, A. M., Rajpalke, M. K., Veal, T. D., Zhukov, A., Robinson, B. J., Anderson, F., Kolosov, O. & Fal'ko, V. Graphitic platform for self-catalysed InAs nanowires growth by molecular beam epitaxy. *Nanoscale Res. Lett.* **9**, 1–7 (2014).
- Koblmüller, G. & Abstreiter, G. Growth and properties of InGaAs nanowires on silicon. *Phys. Status Solidi RRL* **8**, 11–30 (2014).
- Munshi, A. M., Dheeraj, D. L., Fauske, V. T., Kim, D.-C., van Helvoort, A. T., Fimland, B.-O. & Weman, H. Vertically aligned GaAs nanowires on graphite and few-layer graphene: generic model and epitaxial growth. *Nano Lett.* **12**, 4570–4576 (2012).
- Hertenberger, S., Rudolph, D., Becker, J., Bichler, M., Finley, J., Abstreiter, G. & Koblmüller, G. Rate-limiting mechanisms in high-temperature growth of catalyst-free InAs nanowires with large thermal stability. *Nanotechnology* **23**, 235602 (2012).
- Mandl, B., Stangl, J., Hilner, E., Zakharov, A. A., Hillerich, K., Dey, A. W., Samuelson, L., Bauer, G., Deppert, K. & Mikkelsen, A. Growth mechanism of self-catalyzed group III–V nanowires. *Nano Lett.* **10**, 4443–4449 (2010).
- Hong, Y. J., Lee, W. H., Wu, Y., Ruoff, R. S. & Fukui, T. van der Waals epitaxy of InAs nanowires vertically aligned on single-layer graphene. *Nano Lett.* **12**, 1431–1436 (2012).
- Takahashi, K. & Morizumi, T. Growth of InAs whiskers in wurtzite structure. *Jpn. J. Appl. Phys.* **5**, 657 (1966).
- Hong, Y. J., Yang, J. W., Lee, W. H., Ruoff, R. S., Kim, K. S. & Fukui, T. Van der Waals epitaxial double heterostructure: InAs/single-layer graphene/InAs. *Adv. Mater.* **25**, 6847–6853 (2013).
- Wang, G.-C. & Lu, T.-M. *RHEED Transmission Mode and Pole Figures* (Springer, 2014).
- Wu, Y., Hao, Y., Jeong, H. Y., Lee, Z., Chen, S., Jiang, W., Wu, Q., Piner, R. D., Kang, J. & Ruoff, R. S. Crystal structure evolution of individual graphene islands during CVD growth on copper foil. *Adv. Mater.* **25**, 6744–6751 (2013).
- Johansson, J., Wacaser, B. A., Dick, K. A. & Seifert, W. Growth related aspects of epitaxial nanowires. *Nanotechnology* **17**, S355 (2006).
- Larsson, M. W., Wagner, J. B., Wallin, M., Håkansson, P., Fröberg, L. E., Samuelson, L. & Wallenberg, L. R. Strain mapping in free-standing heterostructured wurtzite InAs/InP nanowires. *Nanotechnology* **18**, 015504 (2007).
- Hilner, E., Håkansson, U., Fröberg, L. E., Karlsson, M., Kratzer, P., Lundgren, E., Samuelson, L. & Mikkelsen, A. Direct atomic scale imaging of III–V nanowire surfaces. *Nano Lett.* **8**, 3978–3982 (2008).



This work is licensed under a Creative Commons Attribution 4.0 International License. The images or other third party material in this article are included in the article's Creative Commons license, unless indicated otherwise in the credit line; if the material is not included under the Creative Commons license, users will need to obtain permission from the license holder to reproduce the material. To view a copy of this license, visit <http://creativecommons.org/licenses/by/4.0/>

- Yi, G.-C. *Semiconductor Nanostructures for Optoelectronic Devices* (Springer, 2012).
- Mazid Munshi, A. & Weman, H. Advances in semiconductor nanowire growth on graphene. *Phys. Status Solidi RRL* **7**, 713–726 (2013).
- Kang, M. S., Lee, C.-H., Park, J. B., Yoo, H. & Yi, G.-C. Gallium nitride nanostructures for light-emitting diode applications. *Nano Energy* **1**, 391–400 (2012).

Supplementary Information accompanies the paper on the NPG Asia Materials website (<http://www.nature.com/am>)